Research paper

Anomalous diffusion of single metal atoms on a graphene oxide support

CrossMark

Tom Furnival [a], Rowan K. Leary [a], Eric C. Tyo [b], Stefan Vajda [b], Quentin M. Ramasse [c], John Meurig Thomas [a,*], Paul D. Bristowe [a], Paul A. Midgley [a,*]

[a] Department of Materials Science and Metallurgy, University of Cambridge, 27 Charles Babbage Road, Cambridge CB3 0FS, United Kingdom
[b] Materials Science Division, Argonne National Laboratory, Argonne, IL 60439, USA
[c] SuperSTEM Laboratory, SciTech Daresbury Campus, Keckwick Lane, Warrington WA4 4AD, United Kingdom

ABSTRACT

Recent studies of single-atom catalysts open up the prospect of designing exceptionally active and environmentally efficient chemical processes. The stability and durability of such catalysts is governed by the strength with which the atoms are bound to their support and their diffusive behaviour. Here we use aberration-corrected STEM to image the diffusion of single copper adatoms on graphene oxide. We discover that individual atoms exhibit anomalous diffusion as a result of spatial and energetic disorder inherent in the support, and interpret the origins of this behaviour to develop a physical picture for the surface diffusion of single metal atoms.

© 2017 Elsevier B.V. This is an open access article under the CC BY license (http://creativecommons.org/licenses/by/4.0/).

Determination of the diffusive behaviour of atoms moving across a surface is of fundamental scientific importance and crucial to a better understanding of many surface-related phenomena such as surface phase formation, Ostwald ripening, epitaxial growth and heterogeneous catalysis [1–5]. For example, the realisation that spatially-isolated single atoms [6–9] and nanoclusters [10] offer the potential for highly efficient and selective catalytic reactions warrants greater understanding of their interaction with industrially-relevant substrates, which are often heterogeneous in nature. To date, experimental and theoretical investigations of surface diffusion have tended to focus on model systems such as clean metal surfaces [11,12], while similar studies of catalytically-active systems have been limited. However, the development of detailed models describing the surface diffusion at the atomic scale in these heterogeneous systems is of paramount importance to optimize the stability and reactivity of single-atom catalysts [13]. A system with spatial and energetic heterogeneity is known to result in deviations from the classical model of Brownian motion and can lead to a diverse range of behaviours known as anomalous diffusion [14].

To investigate such diffusive behaviour, it is necessary to track single atom motion over extended time periods, and high resolution (scanning) transmission electron microscopy ((S)TEM) can provide the necessary spatial and temporal resolution [15–19]. Previous (S)TEM work has provided some insight into atom diffusion, e.g. the anomalous diffusion of Fe atoms along a graphene edge [20], but it has often been limited to sequences with just a few atoms and/or insufficient temporal resolution to study the diffusion processes in detail. The limitation arises from a poor signal-to-noise ratio (SNR) in rapidly-acquired (S)TEM images, electron beam damage and the difficulties in tracking atoms accurately.

In this work we have overcome these limitations by using fast STEM imaging coupled with spatio-temporal denoising [21] and robust particle tracking [22] to study the motion of single copper atoms on graphene oxide (GO), using the electron beam to both excite and probe the dynamic behaviour. The metal atom trajectories reflect the heterogeneity of GO, comprising ordered and disordered regions, resulting in both strongly-pinned and highly mobile adatoms. By careful analysis of the STEM data, we find the Cu-GO system exhibits anomalous subdiffusion, and explain this behaviour using a hybrid model combining spatial and energetic disorder.

GO is a form of functionalized graphene, the properties of which can be tuned by controlling the number and type of functional groups, opening up numerous electronic and optical applications [23]. There is also great interest in metal-GO systems for heterogeneous catalysis, with oxygen-containing functional groups acting as preferential pinning sites [24]. GO is known to be spatially heterogeneous with disordered and locally-varying oxygen coverage [25]. Fig. 1a is an annular dark-field (ADF) aberration-corrected STEM image, acquired using a primary electron beam energy of 60 keV, of copper atoms deposited on GO using a customised soft-landing protocol [26]. (The image has been lightly filtered to improve visibility, see Supporting Information.) It is clear

* Corresponding authors.
E-mail addresses: jmt2@cam.ac.uk (J.M. Thomas), pam33@cam.ac.uk (P.A. Midgley).
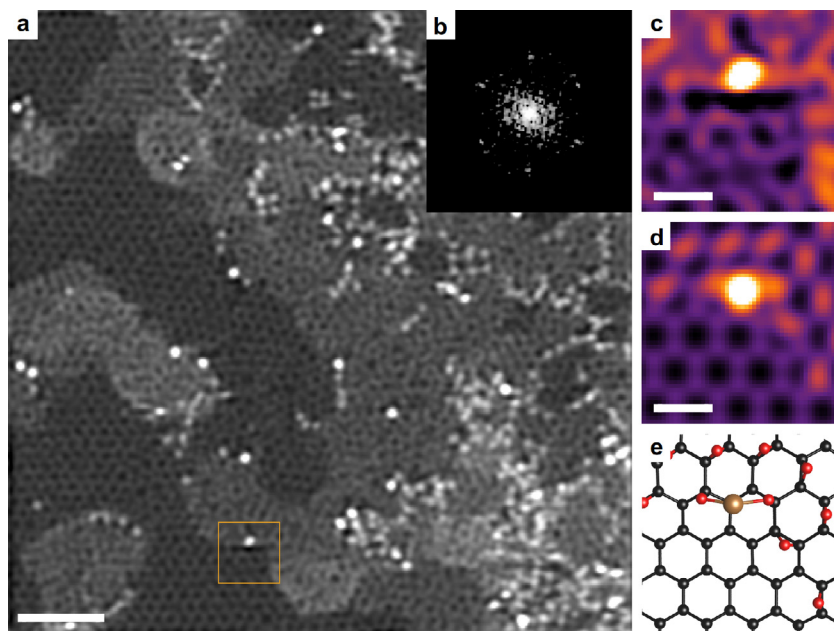
Fig. 1. Heterogeneous structure of graphene oxide. (a) Filtered ADF-STEM image of adatoms on graphene oxide (see methods). Scale bar: 1 nm. (b) Fourier transform of the top-left quarter of the image, showing 6-fold symmetry. (c) Enlargement of the highlighted region, showing the local environment around a copper atom. Scale bar: 0.2 nm. (d) Simulated ADF-STEM image of a structure found with AIRSS, shown in (e). Copper atom is shown in brown, carbon atoms are black and oxygen atoms are red. (For interpretation of the references to colour in this figure legend, the reader is referred to the web version of this article.)

that the GO is a complex material with a number of different environments available for copper adatoms. In agreement with previous (S)TEM studies [27–29], we see relatively pristine graphene regions, with sp^2 character, separated by brighter patches of poorly ordered material, likely to be oxygen-rich and thus exhibiting some sp^3 character (Supporting Information, Fig. S1). Deposited adatoms are seen as bright dots in the image and are found almost universally at the boundaries of the disordered regions, suggesting very strongly that functional groups play a crucial role in the binding of adatoms to the substrate. Analysis of the ADF adatom intensity (Supporting Information) reveals that there are two species: the less bright atoms are silicon impurities; the brighter atoms are copper.

Fig. 1c reveals the local environment around a single copper adatom anchored near the boundary of a disordered oxygen-rich GO region. To gain further insight into the binding of this atom to the underlying GO, we performed a series of density functional theory (DFT) calculations. Fig. S3 in the Supporting Information shows a number of possible low-energy configurations for a copper atom bound to pristine graphene, graphene vacancies and to GO. Copper interacts weakly with graphene, with energy barriers of approximately k_BT at room temperature. This is in line with reported results for other transition metals on graphene [30]. The boundary regions of GO, favoured by the adatoms, were modelled with ab initio random structure searching (AIRSS) [31]. This led to a number of plausible pinning sites with binding energies of ca. 3 eV (Fig. S3). One of these, with binding energy 2.85 eV (Fig. 1e), was used to simulate an ADF-STEM image (Fig. 1d), and shows remarkably good agreement with the experimental image (Fig. 1c). Similar binding energies are also observed for graphene vacancies (Fig. S3), and these too could act as stable pinning sites for Cu atoms.

We investigated the dynamics of copper adatoms on the surface of GO using aberration-corrected STEM, operated at room temperature (T_0) with a primary electron energy of 80 keV, to induce and then image the atomic motion. Such an approach has been used before to probe displacements and dynamics of metal atoms on

graphene supports [32,33], since the electron beam typically provides sufficient energy to excite adatoms out of stable sites and lead to motion across the surface of the support. The maximum energy transferred in a collision by an 80 keV electron to a copper atom is 3 eV (ca. $100k_BT_0$, see Supporting Information), which is sufficient for the electron beam to excite the copper atoms out of the pinning sites explored with DFT in Fig. S3. As well as collisions between the electrons and copper atoms, we note that restructuring of the GO under electron beam irradiation, or an increase in hydrocarbon contamination, may also influence adatom motion.

Two ADF-STEM image sequences were recorded from the same area of the sample with a 40 s wait between the two acquisitions. Each sequence was recorded with a STEM probe size of ca. 0.2 nm, at 8 frames s^{-1}. The estimated dose was 2200 e^- pixel^{-1}, corresponding to a dose rate of 6×10^6 e^- nm^{-2} s^{-1}. Although each individual image in the sequence has a poor SNR, correlations between frames were used to reduce the noise via low-rank matrix recovery [21]. The full sequences are available as Supplementary Movies 1 and 2. Fig. 2a shows a cropped region of sequence 1 after processing, and Fig. 2b is the same region 10 s later. The SNR is still too low to discern the atomic arrangement of the GO substrate, but its graphitic character, and underlying hexagonal symmetry, can be seen following alignment and summation of the frames in each sequence (Supporting Information, Fig. S4). The positions of the copper atoms in each frame were linked to form atomic trajectories; the green track in Fig. 2b shows how a single copper adatom has diffused over 10 s. In total, 63 trajectories were extracted from the two sequences with lengths of 25–130 frames, corresponding to 3–16 s.

Using the trajectories, the diffusive behaviour of the adatoms was explored, starting with the mean squared displacement (MSD) as a function of time, t. Departure from linear behaviour (Brownian motion) leads to superdiffusion or subdiffusion, described by a power-law, MSD $\propto t^\alpha$, where α is the anomalous diffusion exponent. Analysis of the experimental data reveals clear subdiffusive behaviour in both sequences, with $\alpha = 0.50$ for sequence 1 and $\alpha = 0.59$ for sequence 2 (Fig. 2c–d); superdiffusion
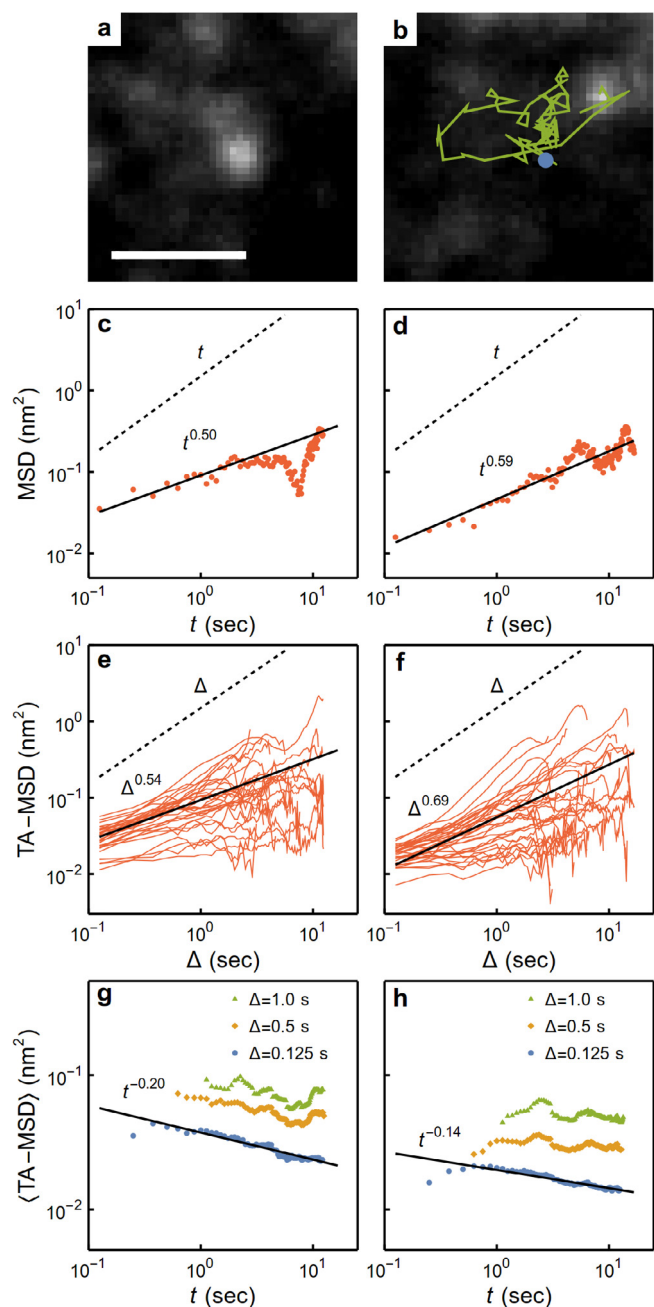
Fig. 2. Anomalous diffusion of copper atoms on graphene oxide. (a) Cropped region from the first frame of sequence 1 after denoising. Scale bar: 1 nm. (b) The same region 10 s later, with a copper atom trajectory highlighted in green. The blue circle highlights the starting position. (c,d) MSD of the trajectories from sequences 1 and 2 respectively. (e,f) TA-MSD of the same trajectories. (g,h) Mean TA-MSD of the trajectories from each sequence as the observation time t increases. For (c–h), best-fit lines are indicated in black with corresponding exponents. (For interpretation of the references to colour in this figure legend, the reader is referred to the web version of this article.)

from Brownian motion is clear with a sub-linear exponent $\beta = 0.54$ for sequence 1 and $\beta = 0.69$ for sequence 2. Furthermore, the trajectories exhibit significant scatter, increasing with Δ, consistent with non-ergodic behaviour since the ensemble and time averages are no longer equivalent. The distribution of the scatter can be plotted to confirm the non-ergodic behaviour (Supporting Information, Fig. S5).

Identifying the physical origin of the observed subdiffusion, and in particular the non-ergodicity, as well as why the subdiffusive behaviour in the two sequences should be subtly different, relies on understanding the models behind anomalous diffusion and how these relate to the experimental system. Common models include the continuous-time random walk (CTRW), where a particle jumps between traps with random dwell times [34]; random walks on fractals, with no characteristic length scales for particle displacements [35]; and fractional Brownian motion (FBM), where the diffusing particle exhibits long-term correlations in displacements [36]. Any model must account for the variety of adatom binding sites, in terms of both relative stability and spatial distribution, as well as the changes in the substrate induced by the electron beam.

From the evidence presented in Fig. 2, ergodic models such as FBM can be ruled out. The CTRW model is a non-ergodic process, and can be related to the experimental system by considering the variation in binding energies of different sites for copper on GO. As the electron beam excites the adatom, it escapes a site with a probability determined by the strength of the binding and the energy transferred by the beam, which is modelled by the random waiting times of a CTRW. The adatom is free to move over the surface until it encounters a new site. A CTRW will also exhibit ageing: as an atom explores the system, it is likely to encounter ever-deeper trapping sites such as vacancies or oxygen-rich regions, and so the observations can depend on the passage of time since the system was created. Atoms initially deposited on weak pinning sites will have diffused to stronger pinning sites by the time the microscopy observations are performed, which is reflected in the notable absence of copper atoms on the pristine graphene regions (Fig. 1a). Averaged over all particles, the mean TA-MSD should show a power-law decay with the measurement time t. For sequence 1, Fig. 2g shows this is indeed the case with an exponent of -0.20; for sequence 2, the exponent has reduced to -0.14 (Fig. 2h).

Although a CTRW model explains many of the anomalous diffusion features, it does not complete the picture. The relationship between TA-MSD and Δ should be linear, rather than the fitted exponents of 0.54 and 0.69. These results and additional analysis (see Supporting Information) point towards a more complex model being required to explain the subdiffusive behaviour. In particular, while a CTRW accounts for energetic disorder in the substrate with a distribution of trapping site energies, it does not incorporate any spatial disorder in the system with pristine graphene alongside disordered regions (Fig. 1a). Instead, the spatial jumps take place either on a regular lattice or are drawn from a normal distribution. Analysis of the particle displacement distributions for various intervals for each sequence (Fig. 3a–b) indicates that this is not the case, with heavy tails and hints of preferred distances due to the underlying GO substrate. Fig. 3c shows, for both sequences, the cumulative distribution of jump lengths, i.e., the likelihood of displacements being larger than a certain value. The data closely follows a log-normal distribution, indicating that the jumps are uncorrelated processes with multiplicative probabilities [37].

Measurements of the electrical conductivity of GO at various levels of oxidation suggests that the spatial disorder in GO can be described using percolation theory [38]. Thus, we propose a combined 'hybrid' model using percolation theory to model the spatial disorder and a CTRW for the temporal disorder to fully describe the
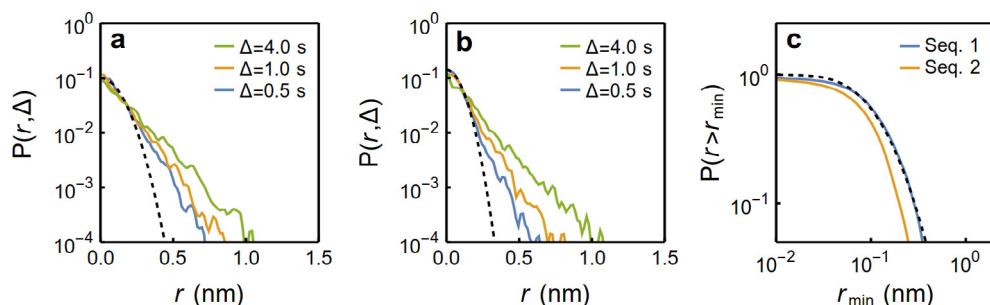
would lead to an exponent greater than 1. Sequence 1 shows hints of a plateau in the MSD at large t, which suggests possible confinement of the adatom motion.

The time-averaged MSD (TA-MSD) represents the mean-squared displacement of each particle in the time interval Δ (see Supporting Information). For Brownian motion the TA-MSD is linear with Δ, and for long measurement times the process is ergodic such that MSD $\simeq$ TA-MSD. The experimental TA-MSDs for each trajectory in each sequence are shown in Fig. 2e–f. The departure

Fig. 3. (a) The distribution of jump lengths, r, at different intervals Δ for sequence 1. The dashed line is a Gaussian fit to the data for $\Delta = 0.5$ s. (b) The same analysis for sequence 2. (c) The cumulative distribution of jump lengths for both sequences, and a fit of a log-normal distribution to sequence 1 (dashed line).

observed anomalous diffusion of single copper atoms on GO. In site percolation, each lattice site is occupied with probability p, taken here as reflecting the fraction of available pinning sites on GO. Unavailable sites in the model correspond to the very heavily oxidized regions of GO (such as seen on the right-hand side of Fig. 1a). These are typically either devoid of Cu adatoms, or have such a high degree of functionalization that the Cu atoms are effectively immobile from the moment they enter the region and so tend to stick to the boundaries. Spatial disorder is incorporated as intermediate values of p, where clusters of accessible sites will exhibit fractal-like characteristics. Atoms undertaking random walks on such clusters will exhibit anomalous diffusion [34].

Fig. 4a shows a simulated random walk on a honeycomb site lattice, with $p = 0.45$ chosen to match the experimental observations in sequence 1 (see Supporting Information for the simulation of sequence 2). Crucially, the ageing behaviour, confirmed experimentally in Fig. 2g, can be replicated only by combining a CTRW with the percolation model (Supporting Information, Fig. S6). When a particle arrives at a lattice site, the waiting time before the next jump is drawn from a power-law distribution as in the CTRW model, which accounts for the stochastic nature of the collisions between accelerated electrons and surface atoms. Particles revisiting a site will have a new waiting time, thus reflecting any beam-induced changes in the substrate that may affect the copper binding energy. The honeycomb lattice incorporates the underlying hexagonal symmetry of the GO, and the possibility of five- and seven-membered rings in defective GO regions is accounted

for by the structural disorder introduced by the site percolation aspect of the model. We stress here that the model illustrated in Fig. 4a is not intended as a direct rendering of the GO lattice, but does incorporate the salient features sufficient to model the experimental observations. Using this hybrid model we match remarkably well the observed subdiffusive behaviour seen in the MSD (Fig. 4b), including a long-time plateau due to confinement (cf. Fig. 2c). Ergodicity breaking is identified by the sub-linear behaviour and scatter in the TA-MSD (Fig. 4c and Supporting Information, Fig. S9), the ageing behaviour (Fig. 4d) and the characteristic jump probabilities (Fig. 4e). Measurement errors in the atom positions and in the trajectory linking are discussed in the Supporting Information. Measurement noise applied to Brownian motion cannot explain the experimental observations (Fig. S10), and noise in the hybrid model needs to be significantly higher than observed before the subdiffusive behaviour is masked (Fig. S11).

Finally, with an understanding of the physical processes involved, we can return to the Cu-GO system and explain the non-ergodic subdiffusive adatom motion in more detail. The electron beam provides sufficient energy for the copper atoms to explore a distribution of binding sites with a range of energies. Adatom movement on sp^2 graphene will be rapid as the binding energies are small. The important binding sites, however, corresponding to the locations of oxygen atoms bound to the underlying graphene, are spatially disordered and can be modelled as a percolation network, and the ageing corresponds to adatoms encountering ever-deeper trapping sites. Although the characteristic
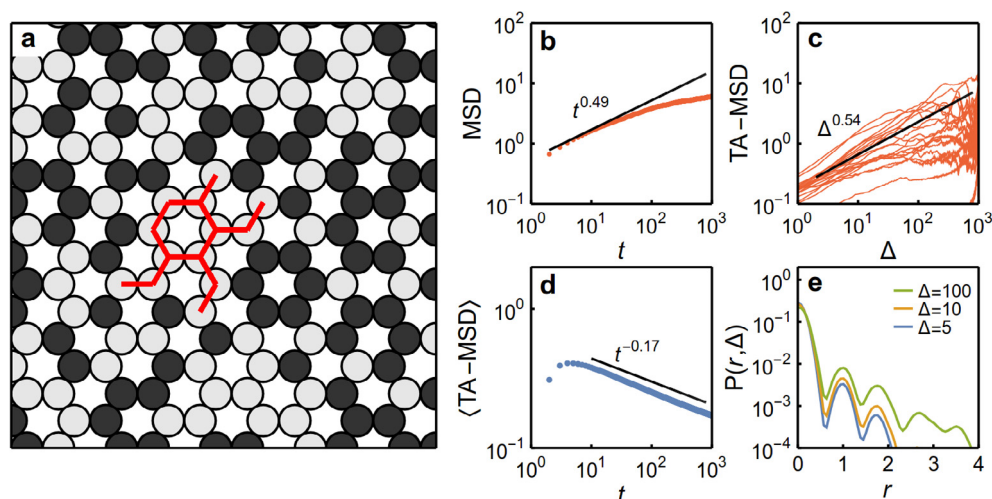

Fig. 4. A model for anomalous diffusion of adatoms on graphene oxide. (a) Honeycomb site lattice with probability of occupancy, $p = 0.47$; grey circles represent available pinning sites, while black circles represent unavailable sites. The red line shows a CTRW on a cluster of available sites. (b) Ensemble MSD, (c) TA-MSD, (d) mean TA-MSD for $\Delta = 1$, and (e) jump length distribution of simulated CTRWs on the lattice. (For interpretation of the references to colour in this figure legend, the reader is referred to the web version of this article.)

behaviour of the adatom motion in sequences 1 and 2 is similar, the subtle differences in ageing and the degree of ergodicity-breaking can be explained by a beam-induced change in the GO support. This could be due to an increase in oxide coverage or hydrocarbon contamination (Supporting Information, Fig. S4). The change leads to a reduction in the area of sp^2 graphene, and thus a reduction in the number of weak binding sites available, and a corresponding increase in the fraction of stronger binding sites to which the adatom may be pinned. Other changes such as the formation of graphene vacancies and the presence of impurity atoms will only increase the variety of available binding sites, further motivating the use of a stochastic CTRW model to account for the adatom binding.

We have used fast atomic resolution STEM imaging to understand the anomalous subdiffusive motion of single copper atoms deposited on graphene oxide using a hybrid CTRW model combined with a site percolation network. This work paves the way towards a more comprehensive understanding, and prediction, of atomic-scale surface diffusion in materials systems possessing spatial and energetic heterogeneity and, furthermore, an improved understanding of the stability and durability of single atom catalysts.

Author contributions

P.A.M. and J.M.T. initiated the project. E.C.T. and S.V. provided the copper samples. R.K.L., T.F. and Q.M.R. performed the STEM experiments. T.F. analysed the data. T.F. and P.D.B. planned and ran the simulations. All authors contributed to writing the manuscript.

Acknowledgements

Appendix A. Supplementary material

Supporting videos, additional details on materials and methods, image analysis, DFT calculations, further tests of anomalous diffusion, discussion on the hybrid model and the effects of measurement error. Supplementary data associated with this article can be found, in the online version, at http://dx.doi.org/10.1016/j.cplett.2017.04.071.

References

[1] G. Antczak, G. Ehrlich, Surface Diffusion: Metals, Metal Atoms, and Clusters, Cambridge University Press, Cambridge, 2010.
[2] D.E. Wolf, J. Villain, Europhys. Lett. 13 (1990) 389–394.
[3] G. Ertl, Reactions at Solid Surfaces, Wiley, Hoboken, N.J., 2009.
[4] M. Copel, M.C. Reuter, E. Kaxiras, R.M. Tromp, Phys. Rev. Lett. 63 (1989) 632–635.
[5] T.R. Johns, R.S. Goeke, V. Asbhbacher, P.C. Thüne, J.W. Niemantsverdriet, B. Kiefer, C.H. Kim, M.P. Balogh, A.K. Datye, J. Catal. 328 (2015) 151–164.
[6] G. Kyriakou, M.B. Boucher, A.D. Jewell, E.A. Lewis, T.J. Lawton, A.E. Baber, H.L. Tierney, M. Flytzani-Stephanopoulos, E.C.H. Sykes, Science 335 (2012) 1209–1212.
[7] X.-F. Yang, A. Wang, B. Qiao, J. Li, J. Liu, T. Zhang, Acc. Chem. Res. 46 (2013) 1740–1748.
[8] J.M. Thomas, Design and Applications of Single-Site Heterogeneous Catalysts, Imperial College Press, London, 2012.
[9] M. Flytzani-Stephanopoulos, Acc. Chem. Res. 47 (2014) 783–792.
[10] E.C. Tyo, S. Vajda, Nat. Nanotechnol. 10 (2015) 577–588.
[11] G.L. Kellog, P.J. Feibelman, Phys. Rev. Lett. 64 (1990) 3143–3146.
[12] G.L. Kellogg, Surf. Sci. Rep. 21 (1994) 1–88.
[13] R. Tromp, Nat. Mater. 2 (2003) 212–213.
[14] R. Metzler, J.-H. Jeon, A.G. Cherstvy, E. Barkai, Phys. Chem. Chem. Phys. 16 (2014) 24128–24164.
[15] A.H. Zewail, J.M. Thomas, 4D Electron Microscopy: Imaging in Space and Time, Imperial College Press, London, 2010.
[16] T.J. Pennycook, L. Jones, H. Pettersson, J. Coelho, M. Canavan, B. Mendoza-Sanchez, V. Nicolosi, P.D. Nellist, Sci. Rep. 4 (2014) 7555.
[17] R. Ishikawa, R. Mishra, A.R. Lupini, S.D. Findlay, T. Taniguchi, S.T. Pantelides, S.J. Pennycook, Phys. Rev. Lett. 113 (2014) 155501.
[18] P.L. Gai, L. Lari, M.R. Ward, E.D. Boyes, Chem. Phys. Lett. 592 (2014) 355–359.
[19] T. Susi, J. Kotakoski, D. Kepaptsoglou, C. Mangler, T.C. Lovejoy, O.L. Krivanek, R. Zan, U. Bangert, P. Ayala, J.C. Meyer, Q. Ramasse, Phys. Rev. Lett. 113 (2014) 1–5.
[20] J. Zhao, Q. Deng, S.M. Avdoshenko, L. Fu, J. Eckert, M.H. Rummeli, Proc. Natl. Acad. Sci. 111 (2014) 15641–15646.
[21] T. Furnival, R.K. Leary, P.A. Midgley, Ultramicroscopy (2016), http://dx.doi.org/10.1016/j.ultramic.2016.05.005.
[22] N. Chenouard, I. Bloch, J. Olivo-Marin, IEEE Trans. Pattern Anal. Mach. Intell. 35 (2013) 2736–3750.
[23] K.P. Loh, Q. Bao, G. Eda, M. Chhowalla, Nat. Chem. 2 (2010) 1015–1024.
[24] X. Chen, G. Wu, X. Chen, Z. Xie, X. Wang, J. Am. Chem. Soc. 133 (2011) 3693–3695.
[25] A. Tararan, A. Zobelli, A.M. Benito, W.K. Maser, O. Stephan, Chem. Mater. 28 (2016) 3741–3748.
[26] C. Yin, E.C. Tyo, K. Kuchta, B. von Issendorff, S. Vajda, J. Chem. Phys. 140 (2014) 174201.
[27] K. Erickson, R. Erni, Z. Lee, N. Alem, W. Gannett, A. Zettl, Adv. Mater. 22 (2010) 4467–4472.
[28] C. Gómez-Navarro, J.C. Meyer, R.S. Sundaram, A. Chuvilin, S. Kurasch, M. Burghard, K. Kern, U. Kaiser, Nano Lett. 10 (2010) 1144–1148.
[29] S. Dave, C. Gong, A. Robertson, J. Warner, J. Grossman, ACS Nano 10 (2016) 7515–7522.
[30] T.P. Hardcastle, C.R. Seabourne, R. Zan, R.M.D. Brydson, U. Bangert, Q.M. Ramasse, K.S. Novoselov, A.J. Scott, Phys. Rev. B 87 (2013) 195430.
[31] C.J. Pickard, R.J. Needs, J. Phys. Condens. Matter. 23 (2011) 053201.
[32] A. Robertson, B. Montanari, K. He, J. Kim, C. Allen, Y. Wu, J. Olivier, J. Neethling, N. Harrison, A. Kirkland, J. Warner, Nano Lett. 13 (2013) 1468–1475.
[33] Z. He, K. He, A. Robertson, A. Kirkland, D. Kim, J. Ihm, E. Yoon, G. Lee, J. Warner, Nano Lett. 14 (2014) 3766–3772.
[34] E.W. Montroll, G.H. Weiss, J. Math. Phys. 6 (1965) 167–181.
[35] D. ben-Avraham, S. Havlin, Diffusion and Reactions in Fractals and Disordered Systems, Cambridge University Press, Cambridge, 2000.
[36] B. Mandelbrot, J.W. Van Ness, SIAM Rev. 1968 (10) (1968) 422–437.
[37] S.M. Tabei, S. Burov, H.Y. Kim, A. Kuznetsov, T. Huynh, J. Jureller, L.H. Philipson, A.R. Dinner, N.F. Scherer, Proc. Natl. Acad. Sci. 110 (2013) 4911–4916.
[38] C. Mattevi, G. Eda, S. Agnoli, S. Miller, K.A. Mkhoyan, O. Celik, D. Mastrogiovanni, G. Granozzi, E. Garfunkel, M. Chhowalla, et al., Adv. Funct. Mater. 19 (2009) 2577–2583.